Investigating the Future Flood and Drought Shifts in the Transboundary Srepok River basin Using CMIP6 Projections

Thanh-Nhan-Duc Tran, Son Kim Do, Binh Quang Nguyen, Vinh Ngoc Tran, Maria Grodzka-Łukaszewska, Grzegorz Sinicyn, and Venkataraman Lakshmi

***Abstract*—Quantifying the intensity and frequency of climatic extremes under the impacts of climate change is crucial for effective water resource management. In this study, we utilize the Soil and Water Assessment Tool (SWAT) hydrological model, robust indices, e.g., Standardized Precipitation Index (SPI) and Standardized Streamflow Index (SSI) as well as the Interquartile Range (IQR) method for a comprehensive analysis of the river flow response to future climate scenarios towards 2090. Four General Circulation Models (GCMs) under two Shared Socioeconomic Pathways (SSPs) have been used, including BCC-CSM2-MR, CanESM5, MIROC6, and MRI-ESM2-0. We aim to reveal the future impacts of extreme events and their potential consequences for local livelihoods and human well-being in the Srepok River basin—a major tributary of the Mekong River basin in Southeast Asia. Our findings include (1) a significant discrepancy between extreme events found with more flood events projected towards 2090; (2) a shift in precipitation patterns with an increase in intensity is observed; and (3) a correlation between climatic extremes and regional characteristics has been identified. This work provides valuable insights into the anticipated changes in climatic extremes under the impacts of climate change and serves as the scientific basis for stakeholders and decision-makers to develop adaptative strategies and sustainable plans to enhance the region's resilience.**

***Index Terms*—Climate change, Drought, Flood, Resilience, Srepok River basin, Mekong River basin, Southeast Asia.**

I. INTRODUCTION

Climate change can considerably impact socioeconomic development, human well-being, and social services worldwide [1], [2], [3], [4], [5]. To address these impacts, the Intergovernmental Panel for Climate Change (IPCC) was established through the joint efforts between the World Meteorological Organization (WMO) and the United Nations (UN). The release of the Sixth Assessment Report (AR6) in 2022 by the IPCC indicates that global mean temperature in the 21st century is anticipated to increase by 1.5 to 2°C compared to the 2020s. Furthermore, it highlights that extreme rainfall events will occur with greater severity and frequency [6]. These changes are predicted to result in the inevitable increases of global extremes (e.g., record-breaking heat waves, widespread floods, year-long droughts, and severe wildfires) [7], anticipating to mark high records [8].

General Circulation Models, also known as Global Climate Models (GCMs), are widely used to quantify projected impacts of future global climate extremes [9], [10], [11]. Version 6 of the Coupled Model Intercomparison Project (CMIP6) introduces the new concept of the Scenario Model Intercomparison Project (ScenarioMIP), which is now based on the Shared Socioeconomic Pathways (SSPs) [12]. This marks a new milestone in the IPCC's effort to incorporate socioeconomic factors [13]. Specifically, SSPs outline potential scenarios for global societal evolution in the future, excluding considerations of climate change and any mitigation or adaptation measures [14]. Each SSP drives a corresponding future projection of greenhouse gas emissions and land cover changes based on its baseline storyline. In addition, ScenarioMIP provides a database essential for water resource inquiries [11], incorporating projected scenarios into hydrological models to enhance our understanding of the physical impact of climate and societal factors on water regimes. However, selecting appropriate CMIP6 GCMs is critical due to various factors such as resolution [15] and geographical characteristics of the region [16].

In this study, we recommend using the NASA Earth Exchange Global Daily Downscaled Projections – NASA NEX-GDDP-CMIP6 (https://registry.opendata.aws/nex-gddp-cmip6/), which has been proven as reliable in previous works [17], [18], [19]. Four CMIP6 GCMs, including BCC-CSM2-MR from the Beijing Climate Center China Meteorological

Manuscript received 31 October 2023; accepted 19 March 2024. Date of publication Date Month 2024; date of current version Date Month YYYY. This study is funded by the Faculty of Building Services, Hydro and Environmental Engineering, and Warsaw University of Technology, Warszawa, Poland, under the representative of Dr. Maria Grodzka-Łukaszewska. (Corresponding author: Thanh-Nhan-Duc Tran). The author Son Kim Do is the co-first author of this work.

Thanh-Nhan-Duc Tran, Son Kim Do, and Venkataraman Lakshmi are with the Department of Civil and Environmental Engineering, University of Virginia, Charlottesville, VA 22904, USA (e-mail: syu3cs@virginia.edu; pgw5jd@virginia.edu; vl9tn@virginia.edu).

Binh Quang Nguyen is with the Faculty of Water Resources Engineering, The University of Danang-University of Science and Technology, Da Nang 550000, Vietnam (e-mail: nqbinh@dut.udn.vn).

Vinh Ngoc Tran is with the Department of Civil and Environmental Engineering, University of Michigan, Ann Arbor, MI 48109, USA (e-mail: vinhtn@umich.edu).

Maria Grodzka-Łukaszewska and Grzegorz Sinicyn are with the Faculty of Building Services, Hydro and Environmental Engineering, Warsaw University of Technology, Warszawa 00-653, Poland (e-mail: maria.grodzka@pw.edu.pl; grzegorz.sinicyn@pw.edu.pl).

Digital Object Identifier 10.1109/JSTARS.2023.xxxxxxx

Administration (China), CanESM5 from the Canadian Centre for Climate Modelling and Analysis (Canada), MIROC6 from the Japan Agency for Marine-Earth Science and Technology and Atmosphere and Ocean Research Institute, The University of Tokyo (Japan), and MRI-ESM2-0 from the Meteorological Research Institute (Japan), have been selected to use in this study. These choices were based on the findings of [20], [21], [22], [23] conducted in global and Southeast Asia case studies. Specifically, [20] and [23] highlighted the usefulness of these GCMs in evaluating future projected streamflow over a river basin in China. [22] demonstrated that CanESM5 and BCC-CSM2-MR have advantages in projecting future precipitation, evapotranspiration, and soil water, compared to the other 11 GCMs. Additionally, [21] identified the highest adaptability in temperature and precipitation of MIROC6 and MRI-ESM2-0, surpassing the other GCMs in a case study in Japan. Besides, IPCC recommended the use of SSP2-45 (intermediate) and SSP5-85 (high-end/extreme) scenarios to quantify different levels of greenhouse gas emissions [6], [21], and socioeconomic characteristics [13], thereby would be used in this work. Specifically, SSP2-45 is an update from the Representative Concentration Pathways (RCP) 4.5 with an additional radiative forcing of 4.5 W/m² by 2100 [13]. This scenario represents the medium pathway of future greenhouse gas emissions, assuming climate protection measures would be applied in the future. Besides, SSP5-85 is constructed as the upper boundary of the highest greenhouse gas emissions, assuming a feasible additional radiative forcing of 8.5 W/m² by the year 2100. This is an update from the previous CMIP5 RCP 8.5 scenario but now incorporates socioeconomic factors.

The Standardized Precipitation Index (SPI) and Standardized Streamflow Index (SSI), which are robust and reliable indices [24], [25], [26], would be used to quantify the projected impacts of climate change on future drought and flood events. While numerical models are commonly used to solve current environmental-related issues [27], [28], [29], [30], [31], [32], [33], [34], it can also be utilized for estimating future impacts of climate [21], [22]. In addition, the Interquartile Range (IQR) method and the Soil & Water Assessment Tool (SWAT) model would be utilized in this work for climate change assessments due to their effectiveness [9], [20], [35].

The Srepok River basin (SRB) is a major tributary of the Mekong River basin (MRB) and contributes a significant volume of water to the Mekong River annually [36], [37], [38]. Changes in the water supply, resulting from climate change, can significantly impact water resource management [39], [40]. This could lead to serious consequences for approximately 11,000 Cambodians living at the SRB's outlet [41].

In summary, this study quantifies the projected changes in future extreme events (2023-2090) using four CMIP6 GCMs with two scenarios each (SSP2-45 and 5-85). We aim to (1) reveal the intensity and frequency changes of extreme events while also (2) quantify the relative contribution of different GCMs to project the trend of these extremes between 2023 and 2090. This work is important for water resource management in local communities in Vietnam and Cambodia. It provides a valuable scientific foundation for disaster prediction and prevention in the lower MRB, thereby supporting stakeholders, regional authorities, and officials.

II. STUDY AREA

The Srepok River is a principal tributary of the MRB, originating from the Dak Lak province in the Central Highlands of Vietnam (Fig. 1a). It flows through Ratanakiri and Stung Treng regions before joining the Mekong River (Figs. 1a and 1b). The river's length varies from 406 to 450 kilometers, with the initial course running through the Vietnamese territory for 125 to 169 kilometers, followed by a 281-kilometer stretch through Cambodian territory [45]. The SRB covers an area of approximately 18,200 km² in Vietnam, with over 65% (12,000 km²) constituting the upper SRB [46].

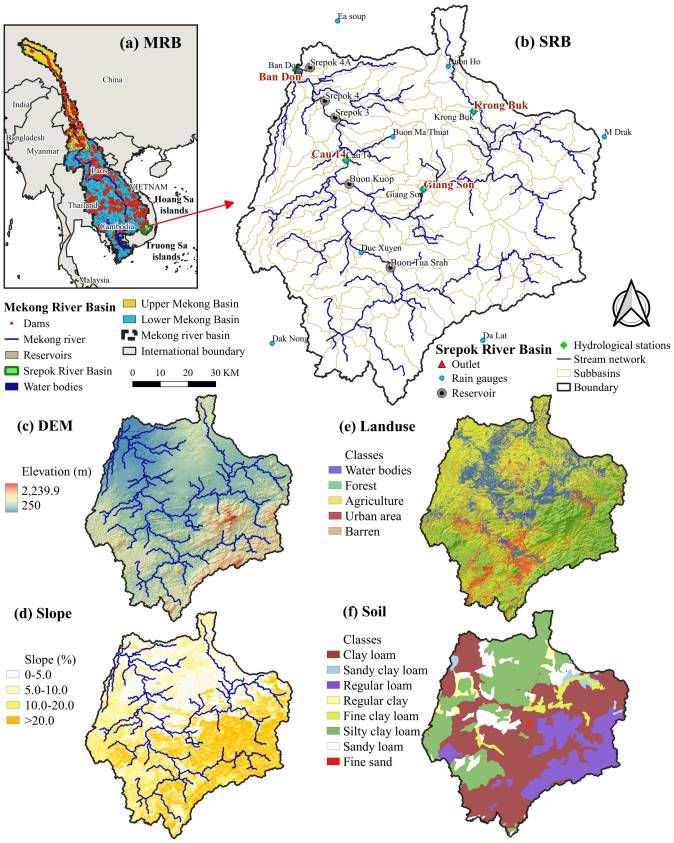

Fig. 1. (a) Location of SRB in the MRB, (b) SRB, (c) DEM (m), (d) Slope (%), (e) LULC map, and (f) Soil type map.

The study region features a complex terrain profile with elevations ranging from 250 to around 2,240 meters (Fig. 1c). While the average altitude of SRB ranges from 350 meters in the Northwest to roughly 1,000 meters in the Southeast [46], [47], the average annual rainfall is found to be approximately 1,920, 1,937, 1,704, and 1,601 millimeters (mm), measured at the Giang Son, Duc Xuyen, Cau 14, and Ban Don stations, respectively. The wet season of the SRB with over 70% of the annual precipitation occurs between June and November, in which approximately 41% of it is converted to direct runoff [46]. In this study, four commissioned reservoirs would also be

included due to their notable impacts on the natural runoff [48], [49], including Buon Tua Srah, Buon Kuop, Srepok 3, Srepok 4, and Srepok 4A [50] (Fig. 1b and Table II).

III. DATA AND METHODS

A. GCMs and Climate Change Scenarios

In this study, we utilized the NASA NEX-GDDP-CMIP6 dataset, which comprises downscaled and bias-corrected GCMs to the resolution of 0.25° x 0.25° (25 x 25 km) [14]. These datasets were downscaled using the Bias-Correction Spatial Disaggregation (BCSD) method, a statistical downscaling algorithm specifically developed to address common limitations of global GCM outputs [51], [52], [53]. The NEX-GDDP-CMIP6 scenarios were produced through the CMIP6 project, focusing on two of the four "Tier 1" greenhouse gas emissions scenarios.

Previous findings have indicated a high uncertainty associated with the individual use of GCMs (e.g., model structure, historical data, projected scenarios, and initial conditions) [54], [55], [56], highlighting the need to use an ensemble of multiple models. Thus, an ensemble model, resulting from the chosen four GCMs, would be utilized for assessments. Moreover, the two greenhouse gas emission scenarios (SSP2-45 and SSP5-85) that represent the intermediate and high-end/extreme levels, respectively, from each GCM were used. The details of GCMs used in this study are presented in Table I.

TABLE I
DETAILS OF THE CMIP6 GCMS USED IN THIS STUDY

No	GCMs	Country	Institution
1	BCC-CSM2-MR	China	Beijing Climate Center China Meteorological Administration
2	CanESM5	Canada	Canadian Centre for Climate Modelling and Analysis, Environment and Climate Change Canada, Canada
3	MIROC6	Japan	Japan Agency for Marine-Earth Science and Technology, Japan & Atmosphere and Ocean Research Institute, The University of Tokyo, Japan & National Institute for Environmental Studies, Japan & RIKEN Center for Computational Science, Japan
4	MRI-ESM2-0	Japan	Meteorological Research Institute, Japan

B. Hydrological model SWAT

SWAT is a semi-distributed hydrological model developed by the U.S. Department of Agriculture (USDA) and Agriculture Research Service (ARS) [57]. In recent years, SWAT has gained popularity in the United States and Europe, mainly due to its effectiveness in addressing hydrological issues [58], [59], [60]. Numerous studies have used the SWAT model to examine the impacts of various factors on streamflow and sediment loads [61], [62]. These factors include changes in land use land cover (LULC) [63], [64], [65], impacts of climate change [9], [66], [67], [68], improvements in ecosystem services [69], [70], [71], validation of satellite-based products [29], [59], [72], [73], [74], [75], [76], and pollution from agricultural chemicals [77].

C. Model inputs

In this study, we used the SWAT hydrological model with the inputs shown in Table II.

TABLE II
DESCRIPTION OF REQUIRED INPUTS FOR SWAT MODEL

No	Name	Description
1	DEM	The DEM (90 m) was retrieved from the HydroSHEDS (V1.0) (https://www.hydrosheds.org/products/hydrosheds) database with an average error of less than 3%.
2	LULC	The 30-m LULC map was retrieved from SERVIR-Mekong program (https://www.landcovermapping.org/en/home/)
3	Soil	The 30-m resampled soil map with from the original scale of 1:1,000,000, extracted from the Food and Agriculture Organization (FAO) (https://www.fao.org/soils-portal/data-hub/soil-maps-and-databases/en/)
4	Weather data	Daily precipitation data were obtained (2001-2018) at eleven meteorological stations, including Giang Son, Buon Me Thuot, Buon Ho, M'DRak, Dak Lak, Krong Buk, Duc Xuyen, Dak Nong, Cau 14, Ban Don, and Ea So (Fig. 1b). Daily maximum temperature (T_{max}) and minimum temperature (T_{min}) data were obtained from the Vietnam meteorological and Hydrological Administration (VMHA) (http://kttvqg.gov.vn/) at two meteorological stations: Buon Me Thuot, and Dak Lak (Fig. 1b).
5	Observation	Observed daily streamflow were collected at five stations: Ban Don, Cau 14, Giang Son, Duc Xuyen, and Krong Buk (Fig. 1b) for the model calibration and validation.
6	Reservoirs	Five dams and reservoirs have been chosen within this study, including Buon Tua Srah with a capacity of 86 Megawatts (MW); Buon Kuop (280 MW), Srepok 3 (220 MW), Srepok 4 (80 MW), and Srepok 4A (63 MW) (Fig. 1b).

D. Model set up

In this study, 2 years (2001 and 2002) were selected as the warm-up period over 18 years of simulation (2001-2018). Nine years (2003-2011) were chosen for model calibration, with validation performed between 2012 and 2018, based on findings from [57]. The calibration and validation of the model were conducted on a daily scale, with the number of iterations set to 500. The Sequential Uncertainty Fitting procedure (SUFI-

2) was chosen as an objective function while the SWAT-CUP program (v5.2.1) was used for the model calibration [78], [79]. The metrics for evaluating the model's performance were presented in Table III, in which we used the Kling-Gupta Efficiency (KGE) [80] and Nash-Sutcliffe Efficiency (NSE) [81].

TABLE III
METRICS USED FOR MODEL PERFORMANCE

[80]	**Criteria**
KGE $= 1 - \sqrt{(CC-1)^2 + \left(\frac{Q_s{}^d}{Q_m{}^d} - 1\right)^2 + \left(\frac{\overline{Q_s}}{\overline{Q_m}} - 1\right)^2}$	VG: KGE ≥ 1; G: 0.50 ≤ KGE ≤ 1; S: 0 ≤ KGE ≤ 0.50; NS: KGE < 0
$NSE = 1 - \frac{\sum_{i=1}^{n}(Q_m - Q_s)^2}{\sum_{i=1}^{n}(Q_m - \overline{Q_s})^2}$	VG: NSE ≥ 0.8; G: 0.8 ≤ NSE ≤ 0.7; S: 0.5 ≤ NSE ≤ 0.7; NS: NSE ≤ 0.5

Q is the streamflow (m^3/s), m and s stand for measured and simulated, respectively, and d stands for deviation, i is the i^{th} measured and simulated, $\bar{Q}$ is the mean value, and number of values is n. VG is Very Good, G is Good, S is Satisfactory, and NS is Not Satisfactory.

In this study, a total of twenty-three parameters were chosen for the calibration and validation of the SWAT model. The sensitivity analysis was conducted using the statistical *p*-value and t-Stat methods [57]. We included the current reservoirs which were neglected in previous works [40], [45], [83], in which two specific parameters were utilized to calibrate these reservoirs, including the hydraulic conductivity of the reservoir bottoms (RES_K; mm/h) and the number of days needed to reach target storage from the current reservoir storage (NDTARGR; days). The SWAT parameters and sensitivity analysis along with their fitted values, descriptions, and ranges can be found in Supplementary section A1.

E. Evaluation indices

Meteorological drought is evaluated through rainfall measurements, while hydrological drought is quantified using streamflow data. This approach provides insights into potential drought-affected areas, based on precipitation levels. However, the drawback of using rainfall anomalies as an indicator is their lack of normalization, making them incomparable across different regions. To address this issue, indices derived from meteorological variables have been developed to monitor and systematically identify dry and wet conditions [84]. In recent decades, a multitude of indices have been introduced, with SPI and SSI standing out as the most prominent [85]. These indices have been widely used in numerous studies, including those by [86], [87], [88]. The severity of drought is assessed based on the selected meteorological variables (e.g., precipitation) and the calculation timescales [89]. The most important feature of the SPI and SSI is their capacity to accurately reflect the timescale-dependent nature of drought phenomena. Specifically, they can be mathematically computed for any timescale, starting from a one-month period. In practical applications, the timescales of 1, 3, 6, 12, and 24 months have proven to be particularly insightful [86]. While a one-month timescale provides a snapshot of the short-term conditions (e.g., short-term soil moisture and crop stress), a three-month timescale offers a seasonal perspective, and a 12-month timescale captures the annual hydrological patterns of rainfall (e.g., changes in reduced streamflow and reservoir storage). The 24-month timescale, on the other hand, is often used in socio-economic studies [22], [90]. In this study, we utilize the 3- and 12-month timescales for SPI (SPI-3 and SPI-12, respectively) to estimate the potential impacts of the seasonal and annual meteorological extreme events.

In this study, SSI was calculated by fitting a specified cumulative probability density function to the extensive daily streamflow data of river channels derived from the SWAT model. Subsequently, this daily streamflow data was transformed into a standard normal distribution to generate the actual SSI series. A prominent advantage of the SSI is its capability to monitor and trace various timescales of hydrological extreme events. Similar to SPI, the short timescales of the SSI, such as the 1- and 3-month scales (SSI-1 and SSI-3, respectively), show a higher sensitivity to short-term hydrological extreme conditions while the longer timescales of the SSI, noted by the 12- and 24-month scales (SSI-12 and SSI-24, respectively), proficiently characterize prolonged hydrological and socioeconomic scenarios. Thus, the 12-month SSI (SSI-12) would be used for our analysis to highlight the inter-annual hydrological conditions using projected streamflow from the SWAT model. The computation of SPI and SSI involved the utilization of daily rainfall and daily simulated streamflow data, from GCMs and the SWAT model, respectively, which were then aggregated to a monthly scale in our analysis.

F. Severity classifications of Climatic Extremes

To accurately evaluate drought and flood conditions, it is important to establish clear criteria for determining the duration and intensity of these events. In this study, we analyzed varying levels of drought and flood severity using the classifications provided by the U.S. Drought Monitor [91]. Specifically, drought conditions are identified when the SPI values fall below zero and continue to decrease to less than negative one (–1). Conversely, a drought event is considered to have ended when the SPI values return to positive while flooding conditions are identified when the SPI values reach positive two (+2) and beyond (Table IV). Based on these criteria, we defined two evaluation indices: Severity (S) and Intensity (ID_e). Specifically, S is calculated as the absolute sum of all SPI values during the event, with the duration defined as the number of months from the onset of the event to its conclusion, excluding the final month when the SPI returns to positive (1). ID_e is calculated as the average SPI value throughout the event

(2). The value of ID_e serves as an indicator of the severity, where higher values indicate more severe conditions. The calculations using SPI and SSI indices would be performed in future periods, including the near future (2023-2044), mid future (2045-2069), and far future (2070-2090).

$$S = \left|\sum_{i=1}^{a} Index_i\right| \quad (1)$$

$$ID_e = \frac{S_i}{a} \quad (2)$$

where a is the duration of the event (months), ID_e is the drought intensity, and S_i represents the SPI or SSI value during the i-month of the event. The frequency (F) of events is calculated as the average number of events during a specified time range.

TABLE IV
SUMMARY OF SPI- AND SSI-BASED SEVERITY CLASSIFICATION

Category	SPI/SSI values
Extreme wet	Index ≥ + 2.0
Severe wet	+ 1.5 ≤ Index < + 2.0
Moderate wet	+ 1.0 ≤ Index < + 1.5
Near normal/mild wet	0 ≤ Index < + 1.0
Near normal/mild drought	- 1.0 ≤ Index < 0
Moderate drought	- 1.5 ≤ Index < - 1.0
Severe drought	- 2.0 ≤ Index < - 1.5
Extreme drought	Index ≤ - 2.0

G. Flood peak assessment using IQR method

IQR serves as a robust measure in statistics, quantifying the dispersion of data within a dataset and aiding in the identification of outliers. By dividing the dataset into quartiles, the IQR offers a general view of data distribution:

- First quartile (Q1): represents the 25th percentile, the median of the dataset's lower half.
- Second quartile (Q2): represents the 50th percentile or the median of the entire dataset.
- Third quartile (Q3): represents the 75th percentile, the median of the dataset's upper half.

In this study, we utilized long-term, daily simulated flood peak simulated from the SWAT model for analysis. We applied the IQR method to perform anomaly detection and find abnormal flood peaks (2023-2090), in which three future periods are defined (see section F). The calculations for IQR and the subsequent identification of outliers will adhere to the equations provided in (3), (4), and (5). This method ensures a systematic and reliable approach to detecting anomalies in flood peak data, ultimately contributing to a comprehensive understanding of potential flood risks in future scenarios.

$$IQR = Q3 - Q1 \quad (3)$$

$$Lower\ bound: Q1 - 1.5\ x\ IQR \quad (4)$$

$$Upper\ bound: Q3 - 1.5\ x\ IQR \quad (5)$$

Data points outside these bounds are considered anomalies, signifying departures from typical flood peak ranges. Specifically, by calculating the IQR across different years and GCMs, we highlight years with exceptionally high and low values, indicating potential risks.

IV. RESULTS AND DISCUSSIONS

A. Model calibration and validation

The most sensitive parameters were found to be SCS runoff curve number (CN2), followed by the base flow alpha factor for bank storage (ALPHA_BNK), the effective hydraulic conductivity in main channel alluvium (CH_K2), manning's "n" value for overland flow (OV_N), plant uptake compensation factor (EPCO), calibration coefficient used to control the impact of the storage time constant from low flow (MSK_CO2), and deep aquifer percolation fraction (RCHRG_DP) [57]. We found that SRB was very sensitive to surface runoff parameters (represented by CN2, CH_K2, and OV_N) and water uptake by plants (EPCO). This could be explained due to the large amount of dense plant cover in the area (e.g., forest and grassland, see Fig. 1e). This finding is consistent with the results from previous studies by [10], [92], [93]. However, groundwater parameters (e.g., RCHRG_DP and GW_DELAY) were found not sensitive in this case, which could be explained by the significant abstraction of groundwater for farming, which reduces the interaction between surface water and subsurface water.

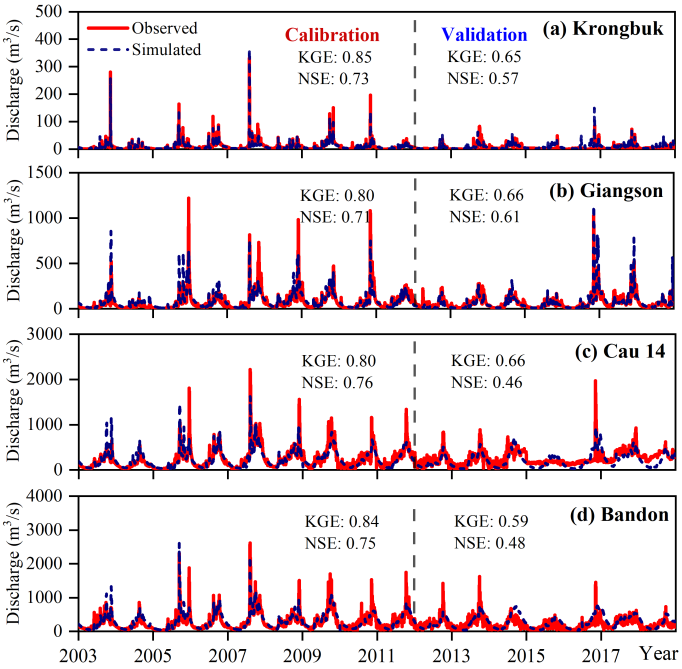

Fig. 2. Comparisons between observed and simulated streamflow on the daily scale at (a) Krongbuk, (b) Giangson, (c) Cau 14, and (d) Bandon, in which calibration (2003-2011) and validation (2012-2018).

The calibration of the model at four stations (2009-2018) yielded good skill scores (Fig. 2). However, due to the operation of new dams and reservoirs, they fell significantly after 2009 which is neglected in [40], [45], [94]. In general, our model performance was categorized as "Satisfactory" (see Table III), particularly when these results were examined under the

cascade impact of these reservoirs. This suggests that the model is reliable for evaluating the climate change impacts in this region.

B. Projected Precipitation and Temperature

First, we analyzed the changes in monthly average temperature and precipitation using GCMs and SSPs (Table V). For future precipitation, there is a noticeable shift in the average monthly precipitation patterns compared to historical data under GCMs and SSP scenarios. Historically, the average monthly precipitation is approximately 127.38 mm. However, this figure is projected at 156.99 mm under the ensemble model SSP2-45, increasing to 160.74 mm (an additional 3.75 mm) in the SSP5-85 scenario (Table V). Besides, other GCMs such as CanESM5 (SSP2-45) and MIROC6 (SSP2-45) show the highest increases of 46.28 mm and 43.20 mm, respectively. Under the SSP5-85 scenario, CanESM5 and MIROC6 indicate potential drought trends, showing decreases of 3.78 mm and 1.26 mm, respectively.

For the maximum temperature, our analysis reveals that while the historical average is around 27.62°C, there are notable variations among GCMs and SSPs. The ensemble model under SSP2-45 projects a significant increase to an average of 32.77°C, a difference of 5.15°C. The SSP5-85 scenario forecasts an additional rise of 0.61°C compared to SSP2-45 (Table V). Besides, individual GCMs predict even higher temperatures; MRI-ESM2-0 in the SSP2-45 scenario shows the highest average maximum at 33.63°C whereas it is 33.99°C for MIROC6 under the SSP5-85 scenario (Table V).

TABLE V

FUTURE PROJECTED CHANGES OF AVERAGE MONTHLY PRECIPITATION AND TEMPERATURE (2023-2090) COMPARED TO HISTORICAL DATA (2003-2018).

MODEL	**TEMPERATURE (°C)**				
	MAXIMUM		TREND	MINIMUM	
	SSP2-45	SSP5-85		SSP2-45	SSP5-85
Ensemble	+ 5.15	+ 5.75	I	+ 5.07	+ 5.67
BCC-CSM2-MR	+ 4.53	+ 5.34	I	+ 5.02	+ 5.59
CanESM5	+ 5.37	+ 6.36	I	+ 5.34	+ 6.33
MIROC6	+ 4.69	+ 5.25	I	+ 4.60	+ 5.24
MRI-ESM2-0	+ 6.00	+ 6.06	I	+ 5.32	+ 5.54
	PRECIPITATION (MM)				
	SSP2-45	SSP5-85	TREND		
Ensemble	+ 29.61	+ 33.36	I		
BCC-CSM2-MR	+ 32.17	+ 36.52	I		
CanESM5	+ 46.28	+ 42.50	D		
MIROC6	+ 43.20	+ 41.95	D		
MRI-ESM2-0	– 3.21	+ 12.47	I		

The positive (+) value represents an increase while the negative (–) value shows a decrease. Trend of models and scenarios are denoted with Increase (I) and Decrease (D).

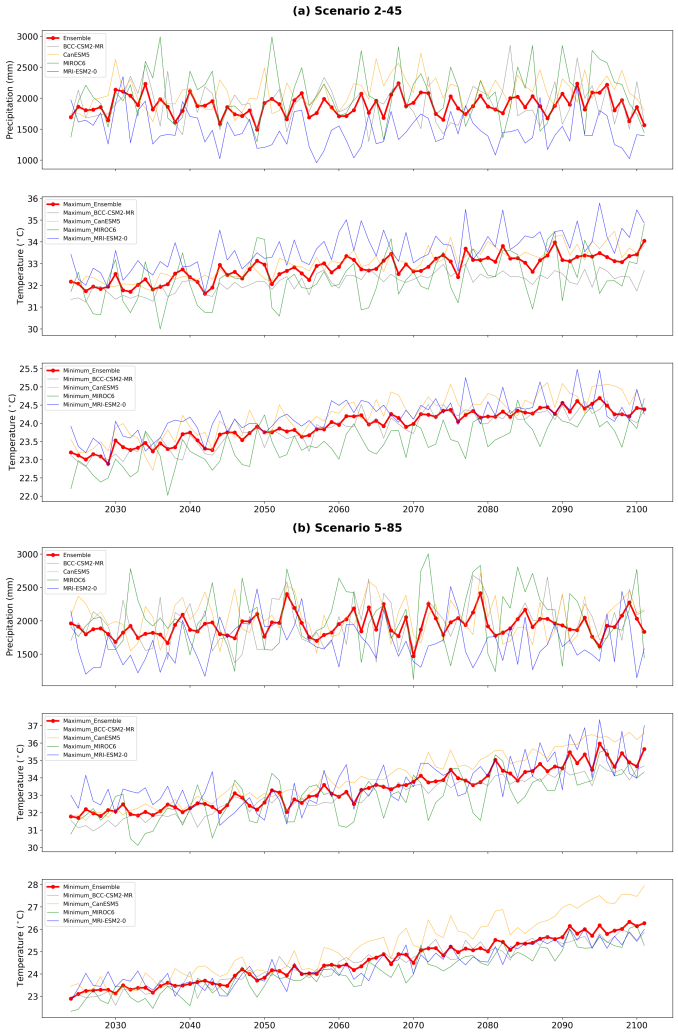

Fig. 3. The average annual precipitation and temperature across GCMs (2023-2100) under (a) SSP2-45 and (b) SSP5-85 scenarios. The red lines represent the ensemble model, which combines the outputs from all GCMs, while other colors show the projections from individual GCMs.

It is noticed that there are projected increases in the average monthly temperature compared to the historical record across various future climate scenarios. Historically, the average minimum monthly temperature is approximately 18.85°C. Under future scenarios, we found an average of 23.92°C (SSP2-45), which then rises slightly to 24.52°C (an additional 0.6°C) under the SSP5-85 scenario (Table V). Among GCMs, MIROC6 shows the lowest increase for both SSP2-45 and SSP5-85 scenarios. In contrast, the CanESM5 model forecasts the highest increases, as 24.19°C and 25.18°C for SSP2-45 and 5-85, respectively. These results indicate a consistent trend of rising temperatures across all models and scenarios (Fig. 3), highlighting the potential for increased drought and flood events, which will be further discussed in the following sections.

C. Evaluation of Future Extremes

We performed our evaluation of extreme events over three different future periods, including the near future (2023-2044), mid

future (2045-2069), and far future (2070-2090) using SPI and SSI indices (see sections E and F). The calculation was performed in seasonal and annual scales (SPI-3 and SPI-12, respectively) under SSP2-45 and 5-85 scenarios.

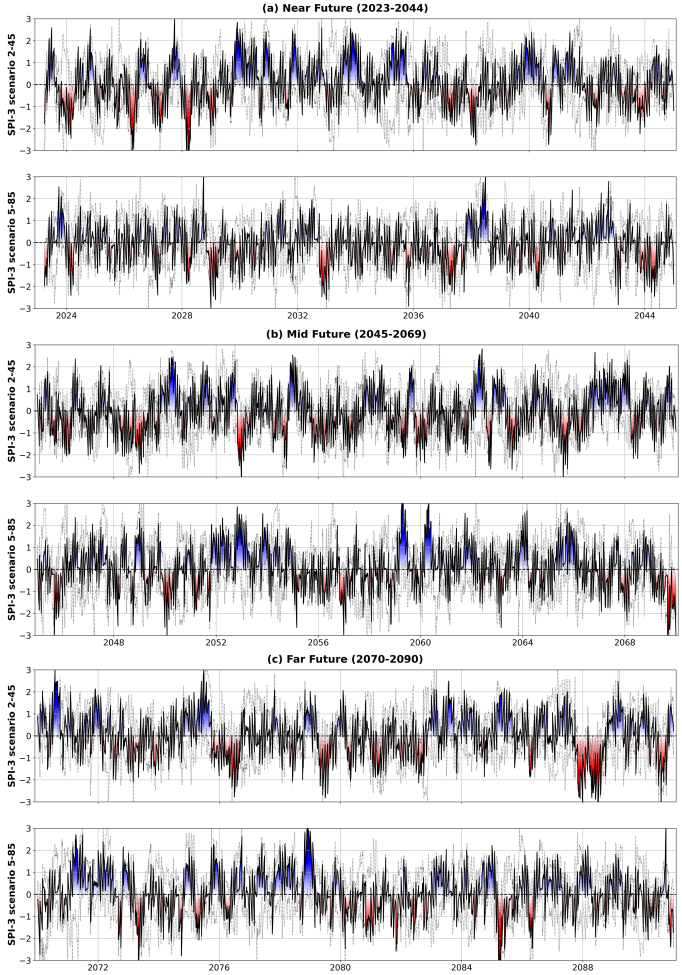

Fig. 4. Evaluation of extreme events using SPI-3 for (a) near future (2023-2044), (b) mid future (2045-2069), and (c) far future (2070-2090). The red color indicates dry periods, while the blue color signifies wet periods. The severity classification is presented in Table IV. The black dotted line represents the SPI-3 range across different GCMs, whereas the red and blue colors denote the values of the ensemble model.

The 3-month SPI (SPI-3) reflects short- and medium-term changes in moisture conditions and the seasonal variations in precipitation anomalies [86]. For SRB, SPI-3 shows significant variability throughout the study period and across different GCMs, as shown in Fig. 4. The dotted lines in the figure represent the range of SPI-3 scores across GCMs and SSPs. For the near future, the SSP2-45 scenario shows a wet condition ($\overline{SPI3_{near}^{2-45}}$ = +0.06), characterized by both significant wet and dry periods in terms of intensity and frequency. Conversely, the scenario SSP5-85 projects a drier condition ($\overline{SPI3_{near}^{5-85}}$ = -0.09). During the mid future (2045-2069), while SSP2-45 shows a slightly drier projection ($\overline{SPI3_{mid}^{2-45}}$ = -0.08), SSP5-85 scenario anticipates more severe and frequent wet trend ($\overline{SPI3_{mid}^{5-85}}$ = +0.07) (Fig. 4b). Lastly, in the far future (2070-2090), neutral to slightly wet conditions are projected in the SRB under both the SSP2-45 and SSP5-85 scenarios ($\overline{SPI3_{far}^{2-45}}$ = -0.001; $\overline{SPI3_{far}^{5-85}}$ = +0.05) (Fig. 5b).

In general, more frequent and pronounced fluctuations between flood and drought conditions are observed in the near and mid future compared to the far future under SSPs, in which SPI values range from +0.06 to -0.09 in the near future and -0.08 to +0.07 in the mid future. However, a contrasting trend is found under the SSP2-45 scenario, in which a shift from a wet to a dry trend is noted, starting with a wet projection in the near future, transitioning to a dry condition in the mid future, and becoming neutral in the far future. In contrast, the SSP5-85 scenario consistently projects a wetter trend, beginning with dry conditions in the near future and progressively becoming wetter in both the mid future and far future (Fig. 4). Additionally, while positive precipitation anomalies (positive SPI-3) are primarily observed in the far future, negative anomalies, indicating short- to medium-term drought periods, become more significant in the near and mid future for both SSP2-45 and SSP5-85 scenarios.

On the other hand, we utilized the SPI and SSI 12-month scale values to better characterize the long-term intensities and durations of droughts and floods for future periods between 2023 and 2090 (Fig. 5). While the SPI-3 is useful for indicating short- to medium-term changes, the SPI-12 and SSI-12 serve as indicators for longer-term meteorological changes, such as the reduction in reservoir levels and groundwater recharge rates [88].

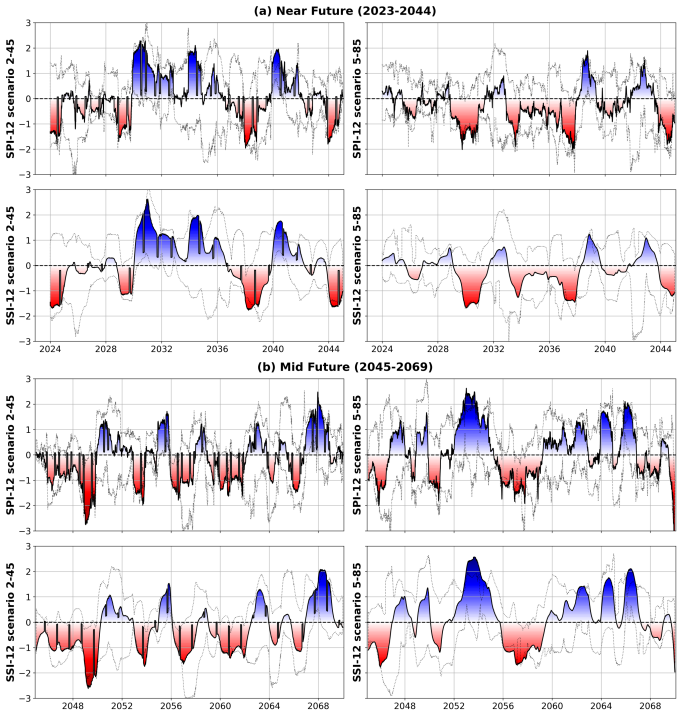

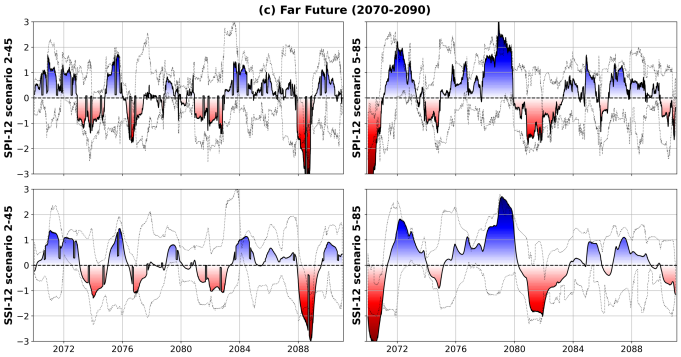

Fig. 5. Evaluation of extreme events using SPI-12 and SSI-12 for (a) near future (2023-2044), (b) mid future (2045-2069), and (c) far future (2070-2090) under the SSP2-45 and 5-85 scenarios. The red color indicates a dry trend, while the blue color signifies a wet trend. The severity classification is presented in Table IV. The black dotted line represents the SPI-12 and SSI-12 range across different GCMs, whereas the red and blue colors denote the values of the ensemble model.

In the near future, SPI-12 (SSP2-45 scenario) suggests a wet trend ($\overline{SPI12_{near}^{2-45}}$ = +0.07), particularly during 2030-2036 and 2040-2042. On the other hand, a predominantly dry trend is found under the SSP5-85 scenario ($\overline{SPI12_{near}^{5-85}}$ = -0.318), with the majority of drought events occurring from 2029 to 2038 (Fig. 5a). For the mid future (2045-2069), the SSP2-45 scenario projects a dry trend ($\overline{SPI12_{mid}^{2-45}}$ = -0.17), with severe droughts spread evenly throughout the period, particularly between 2045-2050 and 2055-2062 (Fig. 5b). In contrast, the SSP5-85 scenario forecasts a significantly wetter trend in the mid future ($\overline{SPI12_{mid}^{5-85}}$ = +0.134), characterized by numerous and prolonged flood events, especially between 2050-2056 and 2060-2067. In the far future (2070-2090), SPI-12 under both SSP scenarios generally shows a mild wet trend ($\overline{SPI12_{far}^{2-45}}$ = +0.04) to a more severe wet condition ($\overline{SPI12_{far}^{5-85}}$ = +0.19) (Fig. 5c). Only a few significant drought periods are observed during this time, specifically around 2076-2077 and 2088-2089 under the 2-45 scenario, and 2070-2071 and 2080-2083 under the 5-85 scenario. In addition, our results reveal that higher greenhouse gas emissions are associated with more severe intensities of both flood and drought events.

Compared to SPI-3, the SPI-12 index shows less temporal variation due to their extended accumulation period, leading to more prolonged meteorological drought and flood periods. While both SPI-3 and SPI-12 show similar trends, suggesting a generally wetter condition, meteorological droughts in the future are anticipated to be both more intense and more frequent. Additionally, under the scenario SSP5-85, both indices indicate a notable increase in flood intensity towards 2090.

The SSI-12 index shows a consistent trend compared to the SPI-3 and 12. Specifically, while longer and more intense drought periods are reflected during the near future ($\overline{SPI12_{near}^{5-85}}$ = -0.21) (SSP5-85) and mid future ($\overline{SPI12_{mid}^{2-45}}$ = -0.28) (SSP2-45), flood trends are found during the near ($\overline{SPI12_{near}^{2-45}}$ = +0.11) (SSP2-45), mid ($\overline{SPI12_{mid}^{5-85}}$ = +0.20) (SSP5-85), and far future ($\overline{SPI12_{far}^{5-85}}$ = +0.14) (SSP5-85) (Fig. 5). Both scenarios consistently project a transition towards a wetter pattern, characterized by increased frequency and extended durations of flood periods (Fig. 5). This notable shift emphasizes the need for strategic planning and adaptive measures to mitigate potential impacts on local ecosystems, infrastructure, and communities.

D. Spatial representation of Future Extremes

In this section, we calculated the average SPI-12 index for 115 subbasins in the SRB, utilizing GCMs and SSP scenarios between 2023 and 2090. This aims to assess projected drought and flood intensities and their spatial representation across the SRB (Fig. 6). A comparative analysis of drought trends using SPI-12 skill scores shows a fluctuating pattern: beginning with a wet trend in the near future ($\overline{SPI12_{near}^{2-45}}$ = +0.06), to a dry projection in the mid future ($\overline{SPI12_{mid}^{2-45}}$ = -0.18), and then stabilizing to a neutral state in the far future ($\overline{SPI12_{far}^{2-45}}$ = +0.03). However, the SSP5-85 scenario consistently indicates a progressively wetter trend across all future periods, suggesting an increase in flooding events, especially in the downstream regions of the SRB (Fig. 6). Specifically, the driest trend is observed in the near future ($\overline{SPI12_{near}^{5-85}}$ = -0.313), while the wettest projection peaks during the far future ($\overline{SPI12_{far}^{5-85}}$ = +0.19).

Both agricultural and urban areas in the SRB (Fig. 1e), are expected to encounter significant flood and drought conditions in the near future. In agricultural regions near Ban Don and Cau 14 stations (see Fig. 1b), mild drought conditions are projected for the mid future under the SSP2-45 scenario. Conversely, under the SSP5-85 scenario, the near future is anticipated to have moderate to severe drought conditions, while the mid and far future are expected to experience mild-to-moderate flood conditions.

In urban areas near Duc Xuyen station and Buon Tua Srah reservoir (Fig. 1b), the SSP2-45 scenario forecasts mild flood conditions for the near future, whereas the SSP5-85 scenario predicts mild to moderate flood conditions in both the mid and far future. These projections emphasize the critical need for flood prevention measures, particularly in the low-lying regions of the SRB (Fig. 1c). In addition, we found that these areas are known for high socioeconomic activities and dense populations [39], [45], thereby our findings aim to support authorities to understand potential impacts of future climate for implementing optimal strategies to maintain human well-being over this region.

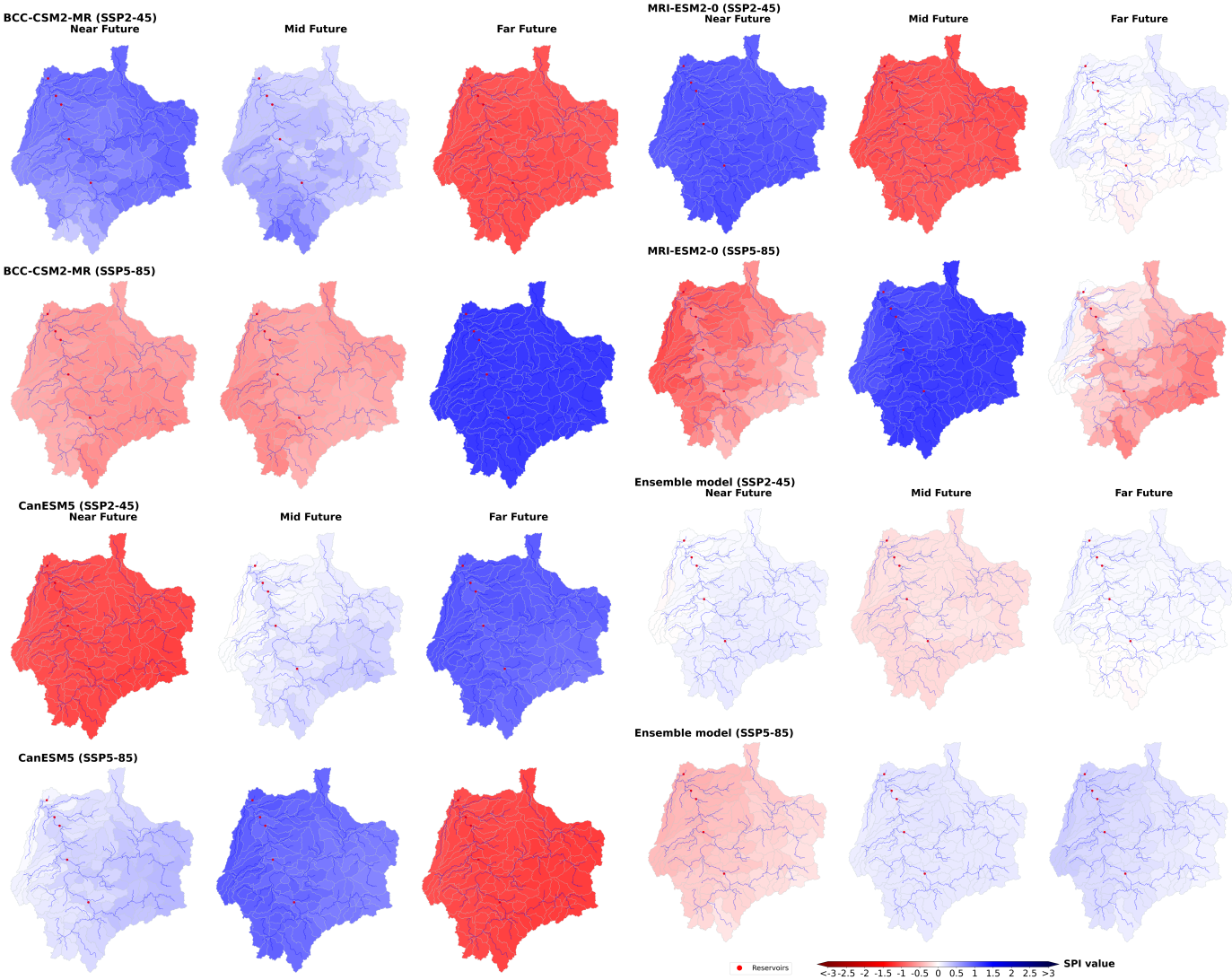

Fig. 6. Spatial representation of the intensity of extremes using SPI-12 over GCMs during the near future (2023-2044), mid future (2045-2069), and far future (2070-2090). The blue color represents the wet trend while the red color represents the dry trend.

We found a correlation between the projected climate trends and the region's characteristics. Specifically, higher elevation areas (Fig. 1c) are projected to experience fewer floods; however, higher intensity of floods is found in the downstream regions (Fig. 6). It is important to note that the near future is projected to see intensified drought conditions. Besides, we found that dense forest regions (Fig. 1c) showed a lower intensity of droughts (Fig. 6), thereby indicating their effectiveness in reducing climatic extremes.

Furthermore, our results indicated that the high-elevation regions with higher slopes contribute to the increase in the risk of severe flooding in downstream regions (Figs. 1d and 6). However, the limitations of the LULC map used in this assessment must be acknowledged. For more accurate future scenario predictions, it would be beneficial to use future

projected LULC maps if applicable. Therefore, these findings should be considered as informative references rather than definitive conclusions.

Additionally, considering the linear relationships observed between drought, flood events, LULC, and soil moisture, we recommend incorporating soil moisture data in future studies. Recent advancements in downscaled soil moisture datasets, as shown in recent works [95], [96], [97], and previously mentioned by [98], offer a valuable source of soil moisture datasets to enhance the accuracy and comprehensiveness of this study. While this section has highlighted the projected drought intensity over future periods, it is important to quantify the frequency of these drought events, which will be addressed in the following section.

E. Drought Frequency

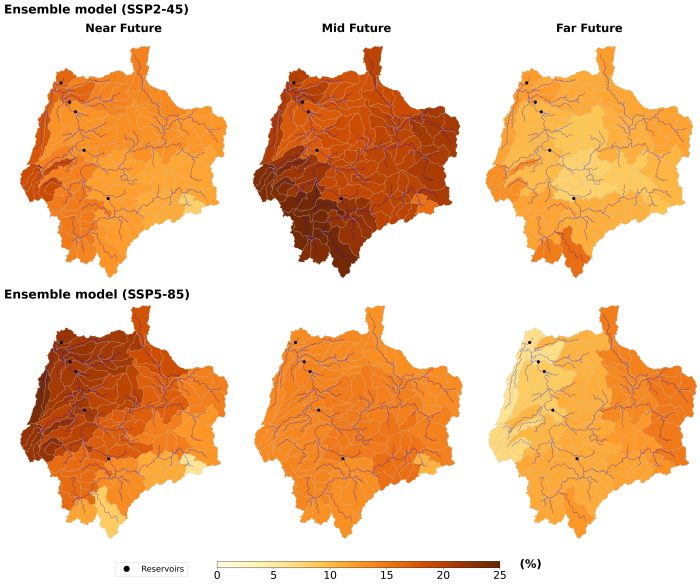

Fig. 7. Spatial representation of drought frequencies using SPI-12 index in the near future (2023-2044), mid future (2045-2069), and far future (2070-2090). The darker color shows a higher probability of drought occurrence.

Fig. 7 shows the spatial representation of drought frequencies. We found that areas within SRB with higher elevations and steeper slopes are especially prone to droughts (Figs. 1 and 7). Furthermore, the outlet region of the SRB is identified as being at a higher risk of both escalating drought occurrences and an increased frequency of flooding events.

G. Projected Streamflow

Understanding projected flood peaks is important in the SRB. Figs. 8 and 9 show the projected flood peaks at the SRB's outlet (Fig. 1b) while Fig. 10 shows the difference in monthly streamflow in percentage, between the baseline scenario and the projections from GCMs and SSPs.

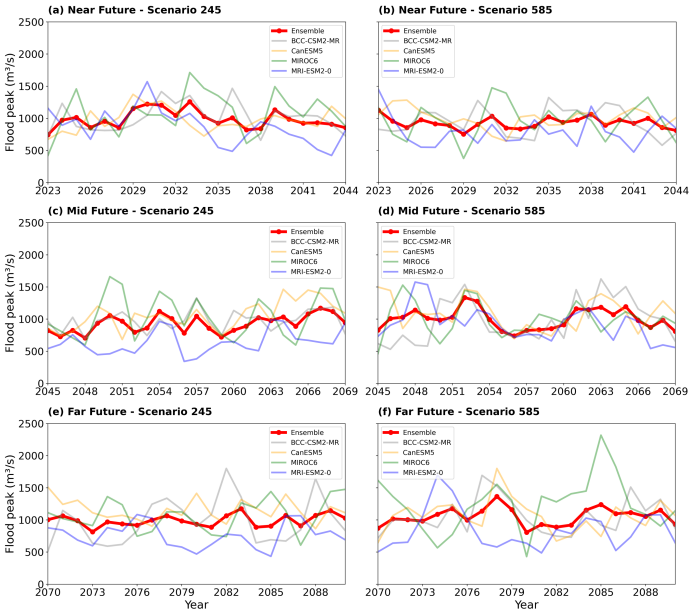

Fig. 8. Projected flood peaks in (a, b) near future (2023-2044), (c, d) mid future (2045-2069), and (e, f) far future (2070-2090) under the SPP2-45 and 5-85 scenarios. The red lines represent the ensemble model, which combines the outputs from all GCMs, while other colors show the projections from individual GCMs.

In the near future (2023-2044), we observed some notable trends among GCMs and SSPs. The ensemble model (SSP2-45) shows high flood peak values, highlighted with the upper bounds formed by the MIROC6 and CanESM5 models (significant in 2028, 2030, 2037, and 2041) and lower bound by the MRI-ESM2-0 model (Figs. 7a and 7b). Interestingly, a decreasing trend of flood peaks is found under the SSP5-85 scenario. Specifically, if we consider the dominant decreasing trend as the main representation over the near future, the lowest difference of -0.19% and the highest difference of -35.66% are found compared to the ensemble SSP2-45. However, while the drying trend is found between 2023 and 2044, the mid future (2045-2069) shows a balanced trend when examining drought and flood years and is consistent with our findings in section C (Fig. 5b). To be specific, under the SSP2-45 scenario, the high-peak return period is found to be between 7 and 9 years, during which the duration of these flooding events ranges from 4 to 5 years. This trend appears similar across GCMs; however, the MIROC6 (SSP5-85) model exhibits a higher number of flooding events compared to other GCMs in the same period (Figs. 8c and 8d).

In the far future (2070-2090), when analyzing projected changes in drought and flood events among GCMs, we found that (1) the wet trend is dominant over the future periods, and higher emissions correlate with more severe flood peaks; (2) the SSP5-85 scenario reveals a consistent extreme drought trend at the beginning of the 2080s (e.g., 2082 and 2083); and (3) while findings from ensemble models are considered more reliable, it is important to note that individual contributions from GCMs

should also be considered, as there can be significant variability in projections. Specifically, MIROC6 (SSP5-85) predicts many significant flooding events, with the lowest difference at 8.06% and the highest at 78.60%, compared to its SSP2-45 counterpart (Figs. 8e and 8f).

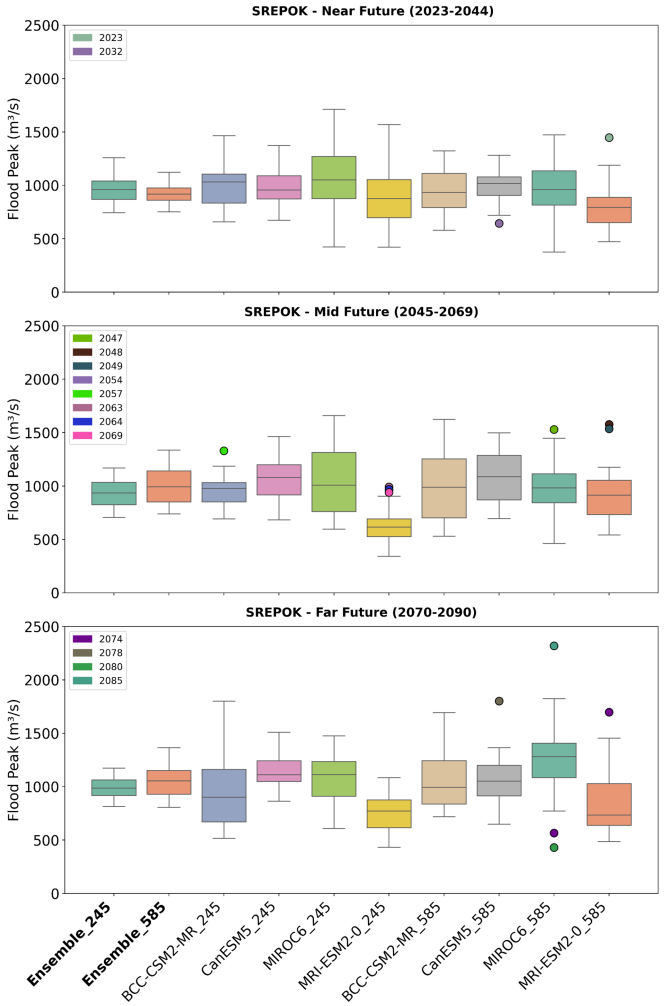

Fig. 9. Temporal anomalies of flood peaks under the SSP2-45 and 5-85 scenarios during the near future (2023-2044), mid future (2045-2069), and far future (2070-2090), utilizing the IQR method.

Anomalously high or low flood peaks can significantly impact hydrological processes [99], ecosystems [100], and human lives [101]. Thus, we utilized the IQR method (see section G) to identify anomalies in flood peaks projected by GCMs and SSPs. In general, we observed an increase in flooding events from the near to the mid future in the SRB (Fig. 9). As discussed in previous sections, the mid future (2045-2069) highlights the transition from dry to wet conditions over SRB. We found that the GCMs exhibit a modest upward shift in median flood peaks across SSPs, with the SSP 5-85 scenario tending to show higher flood peaks. In this assessment, we identified potential peaks projected across GCMs, where the MIROC6 and MRI-ESM2-0 models show significant peaks over the mid and far future (Fig. 9). Specifically, MIROC6 projects a significant high peak in 2047 (1529 m³/s), while MRI-ESM2-0 shows high figures in 2048 (1577 m³/s) and 2049 (1536 m³/s). During the far future, these two models demonstrate extreme high and low peaks; MIROC6 exhibits an extremely high peak of 2319 m³/s, as well as very low peaks in 2074 (566.2 m³/s) and in 2080 (429.7 m³/s). Conversely, MRI-ESM2-0 presents a contrasting extreme high peak in 2074 (1697 m³/s) compared to MIROC6, underscoring the importance of carefully considering these future projections to develop cost-effective strategies and plans.

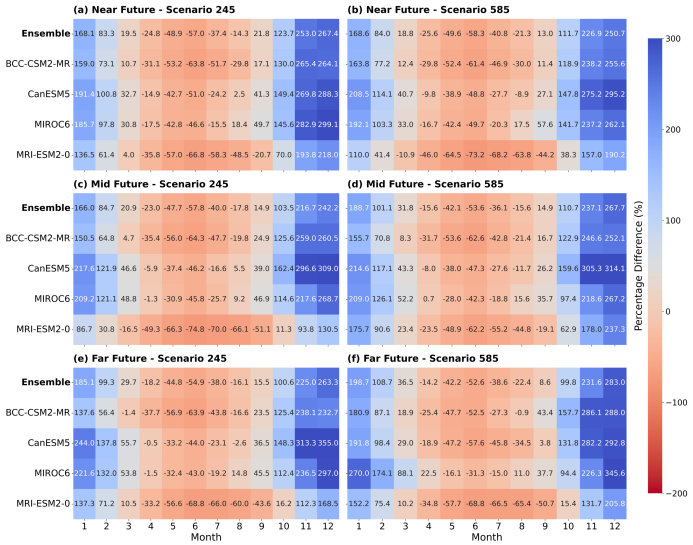

Fig. 10. The monthly streamflow difference in percentage between the historical scenario and GCMs for (a, b) near future (2023-2044), (c, d) mid future (2045-2069), and (e, f) far future (2070-2090) under SPP2-45 and 5-85 scenarios.

Over future periods, the projections for monthly average streamflow show significant variations across GCMs and SSPs. In general, the winter months (December to February) exhibit an increase in streamflow under both scenarios, with the highest records observed in January (Fig. 10). Moreover, the higher emission scenario projects greater intensity, where a high contrast between dry and wet trends is observed towards 2090.

Conversely, our findings reveal that November experiences peaks in average monthly streamflow under the SSP2-45 scenario across GCMs (Figs. 10a, 10c, and 10e). However, under the SSP5-85 scenario, these peaks are shifted to December. The more intense emission scenario (SSP5-85) is associated with a more pronounced increase in streamflow, while the spring and early summer months (April to June) are projected to see a significant decrease in streamflow compared to the historical scenario, with the most notable reduction found in June. These results highlight the severity of the projected extreme events, providing a scientific basis for regional agricultural practice in this region.

V. CONCLUSION

In this study, we conducted a comprehensive analysis to quantify the projected changes in future climatic extremes between 2023 and 2090. Four GCMs from the NASA NEX-GDDP-CMIP6 dataset under two SSP scenarios have been

investigated over three future periods, including the near future (2023-2044), mid future (2045-2069), and far future (2070-2090). Our method included the use of the hydrological SWAT model, robust indices (e.g., SPI and SSI), and IQR method to quantify the intensity and frequency of these climatic events. Our findings are summarized as follows:

(1) A transition from dry to wet conditions is observed towards 2090, with the mid and far future projecting a wetter trend. Notably, the higher emission scenario tends to intensify the severity of climatic extremes. Future projections show a significant discrepancy in the frequency of extreme events towards 2090, accompanied by a shift in monthly precipitation patterns and an increase in intensity.
(2) A shift in average monthly streamflow peaks is observed, transitioning from November to December under the SSP scenarios. The spring and early summer months exhibit a decrease in streamflow compared to historical averages, with the highest figures found in June.
(3) A correlation between future extreme weather events and regional characteristics, such as terrain elevation, slope, and land cover patterns, is indicated. Regions at higher elevations and with dense forest coverage appear to be less susceptible to both drought and flood events.

Our findings provide a scientific basis for understanding the impact of future climatic extremes on the region's water resources. Thus, this work serves as a valuable resource for stakeholders and regional authorities to develop and implement sustainable strategies focusing on disaster prevention in this region.

SUPPLEMENTARY

All supplementary materials have been submitted along with this manuscript.

ACKNOWLEDGMENT

We would like to express our sincere gratitude to anonymous reviewers for their constructive comments to improve the quality of our manuscript. Special acknowledgment also goes to the Faculty of Building Services, Hydro and Environmental Engineering, and Warsaw University of Technology, Warszawa, Poland, for their funding, under the representative of Dr. Maria Grodzka-Łukaszewska.

REFERENCES

[1] M. Marin *et al.*, "Assessing the vulnerability of water resources in the context of climate changes in a small forested watershed using SWATs: A review," *Environ Res*, vol. 184, no. June 2019, 2020, doi: 10.1016/j.envres.2020.109330.

[2] A. Pirnia, H. Darabi, B. Choubin, E. Omidvar, C. Onyutha, and A. Torabi, "Contribution of climatic variability and human activities to stream flow changes in the Haraz River basin, Northern Iran," *Journal of Hydro-environment Research*, vol. 25, no. May, pp. 12–24, 2019, doi: 10.1016/j.jher.2019.05.001.

[3] A. Gädeke *et al.*, "Performance evaluation of global hydrological models in six large Pan-Arctic watersheds," *Clim Change*, vol. 163, no. 3, pp. 1329–1351, Dec. 2020, doi: 10.1007/s10584-020-02892-2.

[4] M. Smigaj *et al.*, "Monitoring riverine traffic from space: The untapped potential of remote sensing for measuring human footprint on inland waterways," *Science of the Total Environment*, vol. 860, no. September 2022, p. 160363, 2023, doi: 10.1016/j.scitotenv.2022.160363.

[5] T.-N.-D. Tran, B. Q. Nguyen, M. Grodzka-Łukaszewska, G. Sinicyn, and V. Lakshmi, "The role of reservoirs under the impacts of climate change on the Srepok River basin, Central Highlands of Vietnam," *Front Environ Sci*, vol. 11, Nov. 2023, doi: 10.3389/fenvs.2023.1304845.

[6] IPCC, "Climate Change 2021: the Physical Science Basis. Contribution of Working Group I to the Sixth Assessment Report of the Intergovernmental Panel on Climate Change," 2021.

[7] B. Q. Nguyen, T. N. D. Tran, M. Grodzka-Łukaszewska, G. Sinicyn, and V. Lakshmi, "Assessment of Urbanization-Induced Land-Use Change and Its Impact on Temperature, Evaporation, and Humidity in Central Vietnam," *Water (Switzerland)*, vol. 14, no. 21, Nov. 2022, doi: 10.3390/w14213367.

[8] IPCC, *Global warming of 1.5°C*. 2019.

[9] M. Shafeeque, M. Hafeez, A. Sarwar, A. Arshad, and T. Khurshid, "Quantifying future water - saving potential under climate change and groundwater recharge scenarios in Lower Chenab Canal, Indus River Basin," *Theor Appl Climatol*, 2023, doi: 10.1007/s00704-023-04621-y.

[10] B. Bhatta, S. Shrestha, P. K. Shrestha, and R. Talchabhadel, "Evaluation and application of a SWAT model to assess the climate change impact on the hydrology of the Himalayan River Basin," *Catena (Amst)*, vol. 181, no. October 2018, p. 104082, 2019, doi: 10.1016/j.catena.2019.104082.

[11] B. C. O. Neill *et al.*, "The Scenario Model Intercomparison Project (ScenarioMIP) for CMIP6," *Geosci Model Dev*, no. April, pp. 1–35, 2016, doi: 10.5194/gmd-2016-84.

[12] V. Eyring *et al.*, "Overview of the Coupled Model Intercomparison Project Phase 6 (CMIP6) experimental design and organization," *Geosci Model Dev*, vol. 9, no. 5, pp. 1937–1958, 2016, doi: 10.5194/gmd-9-1937-2016.

[13] IPPC, "Chapter Outline of The Working Group III Contribution To The IPCC Six Assessment Report (AR6)," 2021. Accessed: Feb. 26, 2024. [Online]. Available: https://www.ipcc.ch/report/ar6/wg3/

[14] B. Thrasher, W. Wang, A. Michaelis, F. Melton, T. Lee, and R. Nemani, "NASA Global Daily Downscaled Projections, CMIP6," *Sci Data*, vol. 9, no. 1, pp. 1–6, 2022, doi: 10.1038/s41597-022-01393-4.

[15] G. Di Virgilio *et al.*, "Selecting CMIP6 GCMs for CORDEX Dynamical Downscaling: Model Performance, Independence, and Climate Change Signals," *Earths Future*, vol. 10, no. 4, Apr. 2022, doi: 10.1029/2021EF002625.

[16] C. Tebaldi *et al.*, "Climate model projections from the Scenario Model Intercomparison Project (ScenarioMIP) of CMIP6," *Earth System Dynamics*, vol. 12, no. 1, pp. 253–293, Mar. 2021, doi: 10.5194/esd-12-253-2021.

[17] B. Thrasher, W. Wang, A. Michaelis, F. Melton, T. Lee, and R. Nemani, "NASA Global Daily Downscaled Projections, CMIP6," *Sci Data*, vol. 9, no. 1, pp. 1–6, 2022, doi: 10.1038/s41597-022-01393-4.

[18] T. Park *et al.*, "What Does Global Land Climate Look Like at 2°C Warming?," *Earths Future*, vol. 11, no. 5, pp. 1–16, 2023, doi: 10.1029/2022EF003330.

[19] T. Yan, J. Bai, T. Arsenio, J. Liu, and Z. Shen, "Future climate change impacts on streamflow and nitrogen exports based on

CMIP5 projection in the Miyun Reservoir Basin, China," *Ecohydrology and Hydrobiology*, vol. 19, no. 2, pp. 266–278, 2019, doi: 10.1016/j.ecohyd.2018.09.001.

[20] C. Chen, R. Gan, D. Feng, F. Yang, and Q. Zuo, "Quantifying the contribution of SWAT modeling and CMIP6 inputting to streamflow prediction uncertainty under climate change," *J Clean Prod*, vol. 364, no. June, p. 132675, 2022, doi: 10.1016/j.jclepro.2022.132675.

[21] S. Peng *et al.*, "Climate change multi-model projections in CMIP6 scenarios in Central Hokkaido, Japan," *Sci Rep*, vol. 13, no. 1, pp. 1–18, 2023, doi: 10.1038/s41598-022-27357-7.

[22] T. Wang, X. Tu, V. P. Singh, X. Chen, and K. Lin, "Global data assessment and analysis of drought characteristics based on CMIP6," *J Hydrol (Amst)*, vol. 596, no. December 2020, p. 126091, 2021, doi: 10.1016/j.jhydrol.2021.126091.

[23] X. Xu *et al.*, "Projected seasonal changes in future rainfall erosivity over the Lancang-Mekong River basin under the CMIP6 scenarios," *J Hydrol (Amst)*, vol. 620, no. PA, p. 129444, 2023, doi: 10.1016/j.jhydrol.2023.129444.

[24] T. Wang, X. Tu, V. P. Singh, X. Chen, and K. Lin, "Global data assessment and analysis of drought characteristics based on CMIP6," *J Hydrol (Amst)*, vol. 596, no. December 2020, p. 126091, 2021, doi: 10.1016/j.jhydrol.2021.126091.

[25] C. Liu, C. Yang, Q. Yang, and J. Wang, "Spatiotemporal drought analysis by the standardized precipitation index (SPI) and standardized precipitation evapotranspiration index (SPEI) in Sichuan Province, China," *Sci Rep*, vol. 11, no. 1, pp. 1–14, 2021, doi: 10.1038/s41598-020-80527-3.

[26] A. R. Salvacion, "Mapping meteorological drought hazard in the Philippines using SPI and SPEI," *Spatial Information Research*, vol. 29, no. 6, pp. 949–960, 2021, doi: 10.1007/s41324-021-00402-9.

[27] T. N. D. Tran, Q. B. Nguyen, and A. Zeeshan, "Application of Plaxis for Calculating the Construction Stability and Soft Embankment in Protecting Ha Thanh," in *2nd Conference on Sustainability in Civil Engineering (CSCE) 2020*, 2021, pp. 202–210. [Online]. Available: https://csce.cust.edu.pk/archive/20-613.pdf

[28] T. N. D. Tran, Z. Ahmed, and N. D. Vo, "APPLICATION OF HYDRODYNAMIC MODELLING TO ASSESS THE EFFICIENCY OF HURRICANE PROTECTION MEASURE AT XOM RO DIKE, PHU YEN PROVINCE, VIETNAM," in *2nd Conference on Sustainability in Civil Engineering (CSCE'20), Department of Civil Engineering Capital University of Science and Technology, Islamabad Pakistan*, 2021. Accessed: Oct. 30, 2023. [Online]. Available: https://csce.cust.edu.pk/archive/20-406.pdf

[29] T. N. D. Tran, Q. B. Nguyen, N. D. Vo, R. Marshall, and P. Gourbesville, "Assessment of Terrain Scenario Impacts on Hydrological Simulation with SWAT Model. Application to Lai Giang Catchment, Vietnam," in *Springer Water*, Springer Nature, 2022, pp. 1205–1222. doi: 10.1007/978-981-19-1600-7_77.

[30] T. Tran *et al.*, "Evaluate the Influence of Groynes System on the Hydraulic Regime in the Ha Thanh River, Binh Dinh Province, Vietnam," in *Advances in Hydroinformatics*, 2022, pp. 241–254. doi: https://doi.org/10.1007/978-981-19-1600-7_15.

[31] T. N. D. Tran, Q. B. Nguyen, T. T. Nguyen, N. D. Vo, C. P. Nguyen, and P. Gourbesville, "Operational Methodology for the Assessment of Typhoon Waves Characteristics. Application to Ninh Thuan Province, Vietnam," in *Springer Water*, Springer Nature, 2022, pp. 887–902. doi: 10.1007/978-981-19-1600-7_55.

[32] V. N. Tran and J. Kim, "Quantification of predictive uncertainty with a metamodel: toward more efficient hydrologic simulations," *Stochastic Environmental Research and Risk Assessment*, vol. 33, no. 7, pp. 1453–1476, Jul. 2019, doi: 10.1007/s00477-019-01703-0.

[33] V. N. Tran, V. Y. Ivanov, D. Xu, and J. Kim, "Closing in on Hydrologic Predictive Accuracy: Combining the Strengths of High-Fidelity and Physics-Agnostic Models," *Geophys Res Lett*, vol. 50, no. 17, Sep. 2023, doi: 10.1029/2023GL104464.

[34] V. N. Tran *et al.*, "A deep learning modeling framework with uncertainty quantification for inflow-outflow predictions for cascade reservoirs," *J Hydrol (Amst)*, vol. 629, Feb. 2024, doi: 10.1016/j.jhydrol.2024.130608.

[35] X. Wan, W. Wang, J. Liu, and T. Tong, "Estimating the sample mean and standard deviation from the sample size, median, range and/or interquartile range," *BMC Med Res Methodol*, vol. 14, p. 135, 2014, doi: 10.1186/1471-2288-14-135.

[36] M. E. Arias, T. Piman, H. Lauri, T. A. Cochrane, and M. Kummu, "Dams on Mekong tributaries as significant contributors of hydrological alterations to the Tonle Sap Floodplain in Cambodia," *Hydrol Earth Syst Sci*, vol. 18, no. 12, pp. 5303–5315, 2014, doi: 10.5194/hess-18-5303-2014.

[37] B. T. Nuong *et al.*, "Applying Fuzzy Analytical Hierarchy Process to Establish Environmental Sustainability Indicators for Water Resources Srepok River Basin , Vietnam," *VNU Journal of Science: Earth and Environmental Sciences*, vol. 38, no. 4, pp. 63–74, 2022.

[38] C. Chang *et al.*, "Operational forecasting inundation extents using REOF analysis (FIER) over lower Mekong and its potential economic impact on agriculture," *Environmental Modelling and Software*, vol. 162, no. August 2022, p. 105643, 2023, doi: 10.1016/j.envsoft.2023.105643.

[39] D. N. Khoi and V. T. Thom, "Impacts of climate variability and land-use change on hydrology in the period 1981-2009 in the central highlands of vietnam," *Global Nest Journal*, vol. 17, no. 4, pp. 870–881, 2015, doi: 10.30955/gnj.001706.

[40] T. Van Ty, K. Sunada, Y. Ichikawa, and S. Oishi, "Scenario-based Impact Assessment of Land Use/Cover and Climate Changes on Water Resources and Demand: A Case Study in the Srepok River Basin, Vietnam-Cambodia," *Water Resources Management*, vol. 26, no. 5, pp. 1387–1407, 2012, doi: 10.1007/s11269-011-9964-1.

[41] International Rivers, "Srepok Dams." [Online]. Available: https://archive.internationalrivers.org/campaigns/srepok-dams

[42] V. Eyring *et al.*, "Overview of the Coupled Model Intercomparison Project Phase 6 (CMIP6) experimental design and organization," *Geosci Model Dev*, vol. 9, no. 5, pp. 1937–1958, 2016, doi: 10.5194/gmd-9-1937-2016.

[43] B. C. O. Neill *et al.*, "The Scenario Model Intercomparison Project (ScenarioMIP) for CMIP6," *Geosci Model Dev*, no. April, pp. 1–35, 2016, doi: 10.5194/gmd-2016-84.

[44] T. L. T. Du *et al.*, "Streamflow Prediction in Highly Regulated, Transboundary Watersheds Using Multi-Basin Modeling and Remote Sensing Imagery," *Water Resour Res*, vol. 58, no. 3, pp. 1–25, 2022, doi: 10.1029/2021WR031191.

[45] T. Van Ty, K. Sunada, and Y. Ichikawa, "A spatial impact assessment of human-induced intervention on hydrological regimes: A case study in the upper Srepok river basin, central highlands of vietnam," *International Journal of River Basin Management*, vol. 9, no. 2, pp. 103–116, 2011, doi: 10.1080/15715124.2011.595720.

[46] T. Van Ty, K. Sunada, and Y. Ichikawa, "A spatial impact assessment of human-induced intervention on hydrological

regimes: A case study in the upper Srepok river basin, central highlands of vietnam," *International Journal of River Basin Management*, vol. 9, no. 2, pp. 103–116, 2011, doi: 10.1080/15715124.2011.595720.

[47] T. Van Ty, K. Sunada, Y. Ichikawa, and S. Oishi, "Scenario-based Impact Assessment of Land Use/Cover and Climate Changes on Water Resources and Demand: A Case Study in the Srepok River Basin, Vietnam-Cambodia," *Water Resources Management*, vol. 26, no. 5, pp. 1387–1407, 2012, doi: 10.1007/s11269-011-9964-1.

[48] N. T. Nguyen *et al.*, "Estimating the Impacts of Ungauged Reservoirs Using Publicly Available Streamflow Simulations and Satellite Remote Sensing," *Remote Sens (Basel)*, vol. 15, no. 18, p. 4563, Sep. 2023, doi: 10.3390/rs15184563.

[49] T. T. P. Bui *et al.*, "Reservoir operation impacts on streamflow and sediment dynamics in the transboundary river basin, Vietnam," *Hydrol Process*, vol. 37, no. 9, Sep. 2023, doi: 10.1002/hyp.14994.

[50] MRC, "The Council Study: The Study on Sustainable Management and Development of the Mekong River Basin, including Impacts of Mainstream Hydropower Projects. Thematic Report on the Positive and Negative Impacts of Hydropower Development on the Social, Environmen," *Mrc*, no. December, p. 107 pp., 2017.

[51] A. W. Wood, E. P. Maurer, A. Kumar, and D. P. Lettenmaier, "Long-range experimental hydrologic forecasting for the eastern United States," *Journal of Geophysical Research: Atmospheres*, vol. 107, no. 20, p. ACL 6-1-ACL 6-15, 2002, doi: 10.1029/2001JD000659.

[52] E. P. Maurer and H. G. Hidalgo, "Utility of daily vs. monthly large-scale climate data: an intercomparison of two statistical downscaling methods," *Hydrol Earth Syst Sci*, vol. 12, pp. 551–563, 2008, doi: 10.5194/hess-12-551-2008.

[53] A. W. Wood, L. R. Leung, V. Sridhar, and D. P. Lettenmaier, "Hydrologic implications of dynamical and statistical approaches to downscaling climate model outputs," *Clim Change*, vol. 62, no. 1–3, pp. 189–216, Jan. 2004, doi: 10.1023/B:CLIM.0000013685.99609.9e.

[54] S. Peng *et al.*, "Climate change multi-model projections in CMIP6 scenarios in Central Hokkaido, Japan," *Sci Rep*, vol. 13, no. 1, pp. 1–18, 2023, doi: 10.1038/s41598-022-27357-7.

[55] C. Chen, R. Gan, D. Feng, F. Yang, and Q. Zuo, "Quantifying the contribution of SWAT modeling and CMIP6 inputting to streamflow prediction uncertainty under climate change," *J Clean Prod*, vol. 364, no. June, p. 132675, 2022, doi: 10.1016/j.jclepro.2022.132675.

[56] Z. Dong, H. Liu, H. Hu, M. Yawar, and A. Khan, "Future projection of seasonal drought characteristics using CMIP6 in the Lancang-Mekong River Basin," *J Hydrol (Amst)*, vol. 610, no. December 2021, p. 127815, 2022, doi: 10.1016/j.jhydrol.2022.127815.

[57] J. G. Arnold *et al.*, "SWAT: Model use, calibration, and validation," *Trans ASABE*, vol. 55, no. 4, pp. 1491–1508, 2012.

[58] P. W. Gassman, M. R. Reyes, C. H. Green, and J. G. Arnold, "The Soil and Water Assessment Tool: Historical Development, Applications, and Future Research Directions," *Trans ASABE*, vol. 50, no. 4, pp. 1211–1250, 2007, doi: 10.13031/2013.23637.

[59] T. N. D. Tran *et al.*, "Quantification of Gridded Precipitation Products for the Streamflow Simulation on the Mekong River Basin Using Rainfall Assessment Framework: A Case Study for the Srepok River Subbasin, Central Highland Vietnam," *Remote Sens (Basel)*, vol. 15, no. 4, Feb. 2023, doi: 10.3390/rs15041030.

[60] T. N. D. Tran *et al.*, "Quantification of global Digital Elevation Model (DEM) – A case study of the newly released NASADEM for a river basin in Central Vietnam," *J Hydrol Reg Stud*, vol. 45, Feb. 2023, doi: 10.1016/j.ejrh.2022.101282.

[61] Z. Ahmed, T. N. D. Tran, and Q. B. Nguyen, "Applying semi distribution hydrological model SWAT to assess hydrological regime in Lai Giang catchment, Binh Dinh Province, Vietnam," in *Proceedings of the 2nd Conference on Sustainability in Civil Engineering (CSCE'20), Capital University of Science and Technology, Islamabad, Pakistan*, 2020, p. 8. [Online]. Available: https://csce.cust.edu.pk/archive/20-404.pdf

[62] B. Q. Nguyen *et al.*, "Response of Hydrological to Anthropogenic Activities in a Tropical Basin," Aug. 2023, pp. 269–278. doi: 10.3850/978-90-833476-1-5_iahr40wc-p1339-cd.

[63] A. Aryal, T. N. D. Tran, K. Y. Kim, H. Rajaram, and V. (Venkat) Lakshmi, "Climate and Land Use/Land Cover Change Impacts on Hydrological Processes in the Mountain Watershed of Gandaki River Basin, Nepal," in *AGU Fall Meeting Abstracts*, Dec. 2022, pp. H52L-0615.

[64] M. Tapas, J. R. Etheridge, G. Howard, V. V. Lakshmi, and T. N. D. Tran, "Development of a Socio-Hydrological Model for a Coastal Watershed: Using Stakeholders' Perceptions," in *AGU Fall Meeting Abstracts*, 2022, pp. H22O--0996.

[65] T.-N.-D. Tran and V. Lakshmi, "The land use changes impacts on socio-economic drivers and simulation of surface and groundwater in the Eastern Shore of Virginia, the United States," in *AGU Fall Meeting Abstracts*, Dec. 2022, pp. H42D-1270.

[66] R. A. Aslam *et al.*, "Integrated SWAT-MODFLOW Modeling-Based Groundwater Adaptation Policy Guidelines for Lahore, Pakistan under Projected Climate Change, and Human Development Scenarios," *Atmosphere (Basel)*, vol. 13, no. 12, p. 2001, 2022, doi: 10.3390/atmos13122001.

[67] M. Shafeeque, Y. Luo, A. Arshad, and S. Muhammad, "Assessment of climate change impacts on glacio - hydrological processes and their variations within critical zone," *Natural Hazards*, vol. 115, no. 3, pp. 2721–2748, 2023, doi: 10.1007/s11069-022-05661-9.

[68] T.-N.-D. Tran *et al.*, "Quantification of Climate Change impacts on the Srepok River, Mekong River basin," *AGU*, 2023, doi: 10.22541/essoar.170365224.48937662/v1.

[69] S. Ashrafi, M. M. M. Khoie, R. Kerachian, and M. Shafiee-Jood, "Managing basin-wide ecosystem services using the bankruptcy theory," *Science of the Total Environment*, vol. 842, no. June, 2022, doi: 10.1016/j.scitotenv.2022.156845.

[70] S. Ashrafi, R. Kerachian, P. Pourmoghim, M. Behboudian, and K. Motlaghzadeh, "Evaluating and improving the sustainability of ecosystem services in river basins under climate change," *Science of the Total Environment*, vol. 806, 2022, doi: 10.1016/j.scitotenv.2021.150702.

[71] M. Behboudian, R. Kerachian, K. Motlaghzadeh, and S. Ashrafi, "Evaluating water resources management scenarios considering the hierarchical structure of decision-makers and ecosystem services-based criteria," *Science of the Total Environment*, vol. 751, 2021, doi: 10.1016/j.scitotenv.2020.141759.

[72] A. Arshad *et al.*, "Reconstructing high-resolution gridded precipitation data using an improved downscaling approach over the high altitude mountain regions of Upper Indus Basin (UIB)," *Science of the Total Environment*, vol. 784, p. 147140, 2021, doi: 10.1016/j.scitotenv.2021.147140.

[73] A. Aryal, T. Tran, B. Kumar, and V. Lakshmi, "Evaluation of Satellite-Derived Precipitation Products for Streamflow Simulation of a Mountainous Himalayan Watershed: A Study of Myagdi Khola in Kali Gandaki," *Remote Sens (Basel)*, vol. 15, no. 19, pp. 47–62, 2023, doi: https://doi.org/10.3390/rs15194762.

[74] R. Noor, A. Arshad, M. Shafeeque, J. Liu, and A. Baig, "Combining APHRODITE Rain Gauges-Based Precipitation with Downscaled-TRMM Data to Translate High-Resolution Precipitation Estimates in the Indus Basin," *Remote Sens (Basel)*, vol. 15, no. 2, p. 318, 2023, doi: 10.3390/rs15020318.

[75] T. N. D. Tran, B. Q. Nguyen, M.-H. Le, V. (Venkat) Lakshmi, J. D. Bolten, and A. Aryal, "Robustness of Gridded Precipitation Products in Hydrological Assessment for Vietnam River basins," in *AGU Fall Meeting Abstracts*, Dec. 2022, pp. H22M-07.

[76] T.-N.-D. Tran, M.-H. Le, R. Zhang, B. Q. Nguyen, J. D. Bolten, and V. Lakshmi, "Robustness of gridded precipitation products for vietnam basins using the comprehensive assessment framework of rainfall," *Atmos Res*, vol. 293, no. 15, p. 106923, 2023, doi: https://doi.org/10.1016/j.atmosres.2023.106923.

[77] S. Chattopadhyay, D. R. Edwards, Y. Yu, and A. Hamidisepehr, "An Assessment of Climate Change Impacts on Future Water Availability and Droughts in the Kentucky River Basin," *Environmental Processes*, vol. 4, no. 3, pp. 477–507, 2017, doi: 10.1007/s40710-017-0259-2.

[78] K. C. Abbaspour, E. Rouholahnejad, S. Vaghefi, R. Srinivasan, H. Yang, and B. Kløve, "A continental-scale hydrology and water quality model for Europe: Calibration and uncertainty of a high-resolution large-scale SWAT model," *J Hydrol (Amst)*, vol. 524, pp. 733–752, 2015, doi: 10.1016/j.jhydrol.2015.03.027.

[79] M. A. Malik, A. Q. Dar, and M. K. Jain, "Modelling streamflow using the SWAT model and multi-site calibration utilizing SUFI-2 of SWAT-CUP model for high altitude catchments, NW Himalaya's," *Model Earth Syst Environ*, vol. 8, no. 1, pp. 1203–1213, 2022, doi: 10.1007/s40808-021-01145-0.

[80] H. V. Gupta, H. Kling, K. K. Yilmaz, and G. F. Martinez, "Decomposition of the mean squared error and NSE performance criteria: Implications for improving hydrological modelling," *J Hydrol (Amst)*, vol. 377, no. 1–2, pp. 80–91, 2009, doi: 10.1016/j.jhydrol.2009.08.003.

[81] D. N. Moriasi, J. G. Arnold, M. W. Van Liew, R. L. Bingner, R. D. Harmel, and T. L. Veith, "Model evaluation guidelines for systematic quantification of accuracy in watershed simulations," *Trans ASABE*, vol. 50, no. 3, pp. 885–900, 2007.

[82] T. D. Tran, V. N. Tran, and J. Kim, "Improving the accuracy of dam inflow predictions using a long short-term memory network coupled with wavelet transform and predictor selection," *Mathematics*, vol. 9, no. 5, pp. 1–21, Mar. 2021, doi: 10.3390/math9050551.

[83] N. T. N. Quyen, N. D. Liem, and N. K. Loi, "Effect of land use change on water discharge in Srepok watershed, Central Highland, Viet Nam," *International Soil and Water Conservation Research*, vol. 2, no. 3, pp. 74–86, 2014, doi: 10.1016/S2095-6339(15)30025-3.

[84] Z. Yu, "Hydrology, Floods and Droughts: Modeling and Prediction," *Encyclopedia of Atmospheric Sciences: Second Edition*, vol. 3, pp. 217–223, 2015, doi: 10.1016/B978-0-12-382225-3.00172-9.

[85] T. B. McKee, N. J. Doesken, and J. Kleist, "The relationship of drought frequency and duration to time scales," in *Proceedings of the 8th Conference on Applied Climatology*, Boston, 1993, pp. 179–183.

[86] A. Docheshmeh Gorgij, M. Alizamir, O. Kisi, and A. Elshafie, "Drought modelling by standard precipitation index (SPI) in a semi-arid climate using deep learning method: long short-term memory," *Neural Comput Appl*, vol. 34, no. 3, pp. 2425–2442, 2022, doi: 10.1007/s00521-021-06505-6.

[87] K. F. Fung, Y. F. Huang, and C. H. Koo, *Assessing drought conditions through temporal pattern, spatial characteristic and operational accuracy indicated by SPI and SPEI: case analysis for Peninsular Malaysia*, vol. 103, no. 2. Springer Netherlands, 2020. doi: 10.1007/s11069-020-04072-y.

[88] L. B. Nguyen, Q. F. Li, T. A. Ngoc, and K. Hiramatsu, "Drought Assessment in Cai River Basin, Vietnam: a Comparison with Regard to SPI, SPEI, SSI, and SIDI," *Journal of the Faculty of Agriculture Kyushu University*, no. 60(2), pp. 417–425, 2015.

[89] J. Sheffield, K. M. Andreadis, E. F. Wood, and D. P. Lettenmaier, "Global and continental drought in the second half of the twentieth century: Severity-area-duration analysis and temporal variability of large-scale events," *J Clim*, vol. 22, no. 8, pp. 1962–1981, 2009, doi: 10.1175/2008JCLI2722.1.

[90] R. Dutta and R. Maity, "Time-varying network-based approach for capturing hydrological extremes under climate change with application on drought," *J Hydrol (Amst)*, vol. 603, Dec. 2021, doi: 10.1016/j.jhydrol.2021.126958.

[91] M. Svoboda *et al.*, "THE DROUGHT MONITOR." [Online]. Available: http://drought.unl.edu/dm

[92] A. R. Bajracharya, S. R. Bajracharya, A. B. Shrestha, and S. B. Maharjan, "Climate change impact assessment on the hydrological regime of the Kaligandaki Basin, Nepal," *Science of the Total Environment*, vol. 625, pp. 837–848, 2018, doi: 10.1016/j.scitotenv.2017.12.332.

[93] C. Li and H. Fang, "Assessment of climate change impacts on the streamflow for the Mun River in the Mekong Basin, Southeast Asia: Using SWAT model," *Catena (Amst)*, vol. 201, no. February, p. 105199, 2021, doi: 10.1016/j.catena.2021.105199.

[94] N. T. Huyen, L. H. Tu, V. N. Q. Tram, D. N. Minh, N. D. Liem, and N. K. Loi, "Assessing the impacts of climate change on water resources in the srepok watershed, central highland of Vietnam," *Journal of Water and Climate Change*, vol. 8, no. 3, pp. 524–534, 2017, doi: 10.2166/wcc.2017.135.

[95] B. Fang, V. Lakshmi, M. Cosh, and C. Hain, "Very High Spatial Resolution Downscaled SMAP Radiometer Soil Moisture in the CONUS Using VIIRS/MODIS Data," *IEEE J Sel Top Appl Earth Obs Remote Sens*, vol. 14, pp. 4946–4965, 2021, doi: 10.1109/JSTARS.2021.3076026.

[96] B. Fang, V. Lakshmi, M. Cosh, P. W. Liu, R. Bindlish, and T. J. Jackson, "A global 1-km downscaled SMAP soil moisture product based on thermal inertia theory," *Vadose Zone Journal*, vol. 21, no. 2, pp. 1–27, 2022, doi: 10.1002/vzj2.20182.

[97] B. Fang, V. Lakshmi, R. Bindlish, and T. J. Jackson, "Downscaling of SMAP Soil Moisture Using Land Surface Temperature and Vegetation Data," *Vadose Zone Journal*, vol. 17, no. 1, pp. 1–15, 2018, doi: 10.2136/vzj2017.11.0198.

[98] B. Fang, P. Kansara, C. Dandridge, and V. Lakshmi, "Drought monitoring using high spatial resolution soil moisture data over Australia in 2015–2019," *J Hydrol (Amst)*, vol. 594, no. July 2020, p. 125960, 2021, doi: 10.1016/j.jhydrol.2021.125960.

[99] E. P. Maurer, G. Kayser, L. Doyle, and A. W. Wood, "Adjusting Flood Peak Frequency Changes to Account for

Climate Change Impacts in the Western United States," *J Water Resour Plan Manag*, vol. 144, no. 3, Mar. 2018, doi: 10.1061/(asce)wr.1943-5452.0000903.

[100] Y. Yin, Y. Wu, S. M. Bartell, and R. Cosgriff, "Patterns of forest succession and impacts of flood in the Upper Mississippi River floodplain ecosystem," *Ecological Complexity*, vol. 6, no. 4, pp. 463–472, Dec. 2009, doi: 10.1016/j.ecocom.2009.08.004.

[101] G. Villarini and J. A. Smith, "Flood peak distributions for the eastern United States," *Water Resour Res*, vol. 46, no. 6, Jun. 2010, doi: 10.1029/2009WR008395.

Thanh Nhan Duc Tran received his Bachelor's degree in Hydraulic Engineering from the Danang University of Science and Technology, Vietnam while received his Joint Master's degree in Hydroinformatics and Water Management from the Université Côte d'Azur (France), the Newcastle University (UK), the Warsaw University of Technology (Poland), the Brandenburg University of Technology Cottbus - Senftenberg (Germany), and the Universitat Politècnica de Catalunya (Spain). He is currently a Ph.D. candidate at the University of Virginia, United States with the focus on Earth Observation and Remote Sensing.

Son Kim Do received his Bachelor's degree in Chemical Engineering from the University of Texas at Austin in 2020 and a Master's degree in Geosensing System Engineering from the University of Houston in 2022. He is currently a Civil Engineering Ph.D. student at the University of Virginia, Charlottesville, Virginia, United States.

Dr. Binh Quang Nguyen is experienced in hydro-sediment-morphodynamics numerical modeling and hydrology. His research interests include quantifying the impacts of dams, land use/land cover changes, and climate change on streamflow, sedimentation, inundation, and morphological evolution.

Dr. Vinh Ngoc Tran received his Bachelor's degree in Hydrology from the Vietnam National University, Hanoi, Vietnam, and received his Ph.D. in Civil Engineering from the University of Ulsan, South Korea. He is currently a Research Fellow at the University of Michigan, Ann Arbor, Michigan, United States.

Dr. Maria Grodzka-Łukaszewska received her Bachelor's and Master's degree in Environmental Engineering in the Faculty of Environmental Engineering, Warsaw University of Technology, Poland. Her PhD which she did in the field of hydrology and water management included issues of numerical modeling of the interaction of surface and groundwater. Currently, he works as an assistant professor at the Faculty of Building Services, Hydro and Environmental Engineering, Warsaw University of Technology (Poland). She is the author or co-author of many publications on surface and groundwater modeling.

Dr. Grzegorz Sinicyn graduated of the Faculty of Sanitary and Water Engineering at the Warsaw University of Technology in 1992. He obtained his PhD in technical sciences in the field of environmental engineering in 1998 at the Faculty of Environmental Engineering of the Warsaw University of Technology. Currently, he is an assistant professor at the Department of Environmental Protection and Management at the Faculty of building Services, hydro and Environmental Engineering of the Warsaw University of Technology. The main topics of his research are modeling of groundwater flow and mass transport in groundwater, the use of Geographic Information Systems (GIS) in environmental protection issues, and hydrology including hydrometry.

Dr. Venkataraman Lakshmi received his Bachelor's degree in Civil Engineering from the University of Roorkee in 1987 and Doctoral degree in Civil and Environmental Engineering from Princeton in 1996. He worked at NASA Goddard Space Flight Center (1996-1999) as a research scientist in the Laboratory for the Atmospheres. He is currently a John L Newcomb Professor of Engineering in the Department of Civil and Environmental Engineering, University of Virginia, USA, the President-Elect of the Hydrology Section of the American Geophysical Union, member of the Water Science and Technology Board, National Academy of Sciences and Vice-Chair of the Earth Science Advisory Committee for NASA, the National Academies Panel for the Decadal Survey of Earth Observations from Space (NASA) and as chair of the planning committee for Groundwater Recharge and Flow: Approaches and Challenges for Monitoring and Modeling Using Remotely Sensed Data (NGA).